Research Article

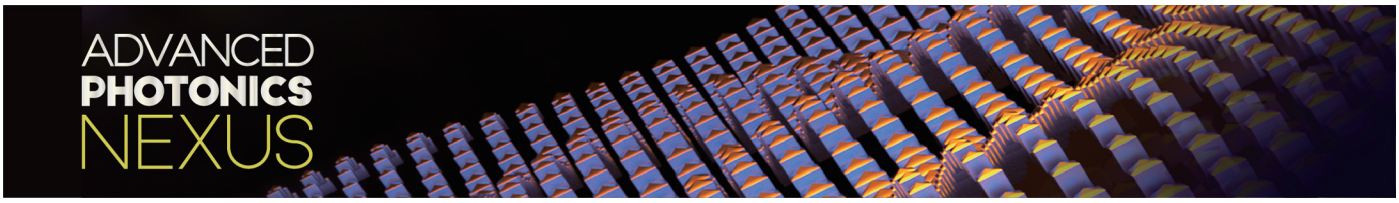

Mode-bases gain difference for different phase profiles in few-mode erbium-doped fiber amplifiers

Jie Zhang,[a,b] Shecheng Gao,[a,*] Wei Li,[c] Jiajing Tu,[a] Yanghua Xie,[a] Cheng Du,[c] Weiping Liu,[a] and Zhaohui Li[b,d]

[a]Jinan University, College of Information Science and Technology, Department of Electronic Engineering, Guangzhou, China
[b]Sun Yat-Sen University, School of Electronics and Information Technology, State Key Laboratory of Optoelectronic Materials and Technologies, Guangzhou, China
[c]Fiberhome Telecommunication Technologies Co. Ltd., Wuhan, China
[d]Southern Laboratory of Ocean Science and Engineering, Zhuhai, China

Abstract. In a few-mode erbium-doped fiber (FM-EDF), which is a key section in a space-division multiplexing (SDM) communication system, linearly polarized (LP) and orbital angular momentum (OAM) modes, as two-mode bases with different phase profiles, can be transformed into each other. In principle, the LP and OAM modes have a different mode spatial intensity distribution and a gain difference for FM-EDF amplifiers. How to analyze and characterize the differential mode-bases gain (DMBG) is important, but still an issue. We build, for the first time to our knowledge, a local analysis model composed of discrete elements of the FM-EDF cross section in areas of mode spatial intensity distribution azimuthal variation. Using the model of the two mode bases, analysis of local particle number distribution and detailed description of the local gain difference are realized, and the overall gain difference between the two mode bases is obtained. By building an amplifier system based on mode phase profile controlling, the gain of two mode bases is characterized experimentally. The measured DMBG is ~0.8 dB in the second-order mode, which is consistent with the simulation result. This result provides a potential way to reduce the mode gain difference in the FM-EDF, which is important in improving the performance of the SDM communication system.

Keywords: space-division multiplexing; few-mode erbium-doped fiber amplifier; linearly polarization; orbital angular momentum.

Received Feb. 24, 2024; revised manuscript received Oct. 21, 2024; accepted for publication Dec. 4, 2024; published online Jan. 17, 2025.

© The Authors. Published by SPIE and CLP under a Creative Commons Attribution 4.0 International License. Distribution or reproduction of this work in whole or in part requires full attribution of the original publication, including its DOI.

[DOI: 10.1117/1.APN.4.1.016007]

1 Introduction

Mode-division multiplexing (MDM) in few-mode fibers (FMFs) is a form of space-division multiplexing (SDM) communication system[1–4] in which multiple modes are used to transmit multiple independent data streams. This approach has been widely investigated and applied to solve the capacity crunch problem of optical fiber transmissions using signal mode fibers.[5–7] With the development of MDM technology, the number of multiplexed channels in fibers has proliferated.[8–12] As a critical device in the FMF-MDM communication system, a few-mode erbium-doped fiber amplifier (FM-EDFA)[13–15] is the most commonly used to improve the transmission distance, but it must be redesigned and upgraded to ensure mode gain equalization[16–18] and to increase the saturated output power. In the past research, FM-EDFAs have been employed to realize mode gain equalization through the following three main strategies: changing the mode field intensity by designing a special refractive index profile,[19] managing the spatial distribution of the doped erbium ions,[20] and controlling the pump mode.[21,22] A lower differential mode gain (DMG, maximum difference of gain for a particular wavelength among different signal modes[23]) requires a more complex pump mode superposition, a multilayer erbium doping distribution, or a special refractive index profile. The DMG of the FM-EDFA is the most pressing problem to be solved because it limits both the capacity and reach of the MDM transmission.[24,25] Similarly,

*Address all correspondence to Shecheng Gao, gaosc825@163.com

increasing the saturated output power is another challenge in the practical application of FM-EDFAs. Through erbium ytterbium codoping,[26] pumping collectors[27] and cladding pumps can increase the saturated output power of FM-EDFAs. However, all the above-mentioned solutions place high requirements on the manufacturing process of few-mode erbium-doped fibers (FM-EDFs). Therefore, it is necessary to seek a solution with a simple fiber structure design and easy manufacturing process to realize mode gain equalization and increase the saturated output power of FM-EDFAs.

Two spatial mode bases are generally available in FMF-MDM systems: orbital angular momentum (OAM) mode[28–31] and linear polarization (LP) mode.[32–34] The LP and OAM modes can be transformed into each other and formed by a degenerate linear combination of the vector modes[35,36] in FMFs. The modal field intensity distributions of the LP and OAM modes exhibit different shapes in space.[37] In effect, the mode spatial intensity distribution determines the spatial distribution of photons and thus the gain of FM-EDF. A differential mode-bases gain (DMBG) exists in the amplification process due to differences in mode spatial intensity distribution between the OAM and LP modes within the same order of the vector mode group.[38–40]

The underlying reasons leading to DMBG between LP and OAM modes are as follows. In LP mode bases, the angular fluctuation of the signal light intensity distribution corresponds to the great difference in the angular distribution of the induced photon number during the amplification process, and the situation occurs that the regions with strong light intensity reach saturation gain, whereas the excited ions in the weak regions cannot be fully utilized. In OAM mode bases, this situation does not occur because the signal light intensity is evenly distributed along the angular direction. Therefore, by controlling the mode phase profile,[39,41,42] the amplified mode bases in FM-EDFAs can switch between the LP and OAM modes to generate DMBG, which can be utilized to dynamically adjust the DMG. In contrast to the DMBG, the DMG in FM-EDF mainly stems from the gain difference among mode groups. This is because the intensity distribution of each mode under the same mode basis in the same mode group is almost uniform, and thus, the gain difference is often negligible.[15,43] In addition, the OAM mode bases can be used to increase the saturated output power of FM-EDFAs in different order modes. This strategy can improve the performance of FM-EDFAs without needing to adjust the structure of the active fiber or control pump mode, such as the core pump mode or cladding pump. However, the cause of DMBG generation between the LP and OAM modes has not been systematically investigated in FM-EDFAs.

In this paper, for the first time to our knowledge, a discrete pixelated local analysis model for FM-EDF is constructed to accurately characterize the local gain of signal mode in detail and then obtain the overall mode gain difference between two mode bases. The difference between LP and OAM mode bases in the amplification process of FM-EDFA is mainly derived from the difference in the distribution of their mode intensity. This is because the different mode spatial intensity distributions determine the spatial photon number distribution, the spatial distributions of the number of erbium ions in the excited state and the ground state are determined by the spatial distribution of signal light photon numbers, and the overall gain of the signal mode is then determined. Based on the proposed local analysis model, through theoretical analysis and numerical simulation, we discover that for the same order azimuthal mode with an input signal power ranging from −15 to 15 dBm, the DMBG falls between 0.37 and 0.95 dB. By building an amplifier testing system based on controlling the mode phase profile, the experimental results show that for the same-order modes with an input signal power of −10 dBm, the first- and second-order DMBGs are 0.40 and 0.80 dB, respectively. Then, we use DMBG to realize mode gain equalization, which changes the DMG from 1.72 to 1.32 dB and increases the saturated output power. The experimental results are consistent with the simulation results, demonstrating the influence of the phase profile on the gain difference of the FM-EDFA. The mode-bases switching method based on controlling the mode phase profile can be used to achieve a smaller DMG and to increase the saturation output power to improve the performance of the SDM communication system in the experiment.

2 Theoretical Model Analysis

Under the weak guide approximation condition of traditional FMFs, both the LP and OAM modes have the same order vector mode group, and they can be deduced from each other. OAM modes can be obtained by combining degenerate odd and even LP modes with a $\pi/2$ phase difference.[44,45] In general, the LP and OAM modes are derived from degenerated vector modes (eigenmodes) in the FMF for their weakly guiding structure.[46] There exist four vector modes ($TE_{0,1}$, $HE_{2,1}^{even}$, $HE_{2,1}^{odd}$, $TM_{0,1}$ for $l = 1$, and $HE_{l+1,1}^{even}$, $HE_{l+1,1}^{odd}$, $EH_{l-1,1}^{odd}$, $EH_{l-1,1}^{odd}$ for $l > 1$, where l is the azimuthal order index) with almost similar n_{eff} for any high-order azimuthal modes, which comprise a single mode group, as shown in Fig. 1(b).[36,38] Due to the almost similar n_{eff}, in a traditional FMF, the stable mode patterns are usually presented in the form of the linear combination of the degenerate vector modes, namely, LP or OAM modes. The resultant intensity distributions, along with schematic representations of n_{eff} for the first two high-order azimuthal modes in two mode bases, are shown in Figs. 1(a) and 1(c). In principle, the modes in any base can be yielded by a linear combination of modes in the other bases.[36,47] The relationship among the three mode bases of the LP, vector, and OAM modes can be seen in Fig. 1. Although these mode bases are mutually unbiased and the modes can be linearly combined with each other in different bases, the mode intensity profile is significantly different in different bases due to the different mode phase distribution determined by the combination form, as shown in Figs. 1(a) and 1(c).

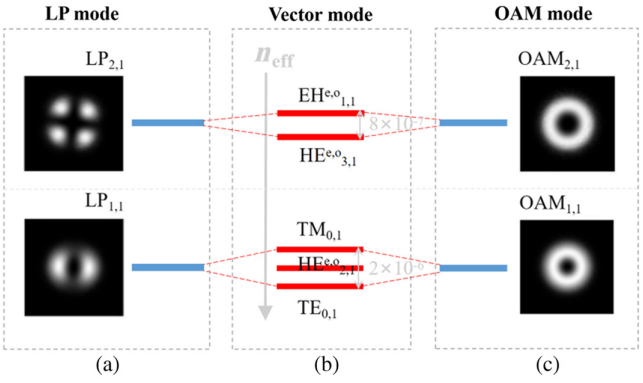

Fig. 1 The first- and second-order azimuthal mode bases of few-mode fibers in the (a) LP mode, (b) full vector mode, and (c) OAM mode.

This intensity profile difference must be taken care of because it provides a way to adjust the DMG among different mode groups by switching the mode bases through the phase distribution. The phase distribution corresponding to the different modes is formed by the different superposition of the same group vector modes.[36] The mode phase distribution and its changes can be realized by the combination of excited modes in the FMF, and this combination is determined by the phase distribution and polarization state of the launched light.

When analyzing DMBG with different phase profiles, we need to consider the mode propagation stability in optical fibers.[47] Various random disturbances will be encountered in long-distance optical fiber communication transmission systems, resulting in poor mode stability[48] and mode bases switching between the LP mode and OAM mode. The mode propagation stability is critical during short-distance optical fiber communication transmission systems, especially in the active fiber length range (usually on the order of several meters, e.g., ~3 m in this work). The OAM mode may be taken as a combination of several vector modes with different propagation constants. Taking $\mathrm{EH}_{l-1,1}^{\mathrm{odd}} + i\mathrm{EH}_{l-1,1}^{\mathrm{even}}$ as an example, the electric field of $E(\xi, z)$ should be[49]

$$E(\xi, \mathrm{z}) = \left[\hat{\sigma}^{+}\mathrm{OAM}_{-l}\cos\left(\frac{\beta_1-\beta_2}{2}z\right) + i\hat{\sigma}^{-}\mathrm{OAM}_{+l}\sin\left(\frac{\beta_1-\beta_2}{2}z\right)\right]e^{i\frac{\beta_1+\beta_2}{2}z}, \quad (1)$$

where β_1 and β_2 are the propagation constants (this can also be characterized by an effective index of the mode given by $n_{\mathrm{eff}} = \lambda\beta/2\pi$) of the odd and even modes in one mode group. With the combination of odd and even modes with different propagation values, the topological charge l of the OAM mode periodically changes with the propagation distance, and its cut-off length $Z_{\mathrm{walk-off}} = \pi/(\beta_1 - \beta_2) = \lambda/2\Delta n_{\mathrm{eff}}$ will decrease by increasing the difference in effective refractive index Δn_{eff} of the odd and even modes. The active fiber used in the experiment was chosen as an example at a wavelength of 1550 nm, and the Δn_{eff} calculated using a finite-element method is $\sim 6.3 \times 10^{-11}$ ($\mathrm{HE}_{2,1}^{\mathrm{odd}}$ and $\mathrm{HE}_{2,1}^{\mathrm{even}}$), 1.1×10^{-11} ($\mathrm{EH}_{1,1}^{\mathrm{odd}}$ and $\mathrm{EH}_{1,1}^{\mathrm{even}}$), 2.6×10^{-11} ($\mathrm{HE}_{3,1}^{\mathrm{odd}}$ and $\mathrm{HE}_{3,1}^{\mathrm{even}}$), $<3.0 \times 10^{-14}$ between the odd and even modes in the LP mode bases, and $<5.8 \times 10^{-11}$ between the $+l$ and $-l$ modes in the OAM mode bases, respectively. Among them, the resulting minimum $Z_{\mathrm{walk-off}}$ is $\sim 1.23 \times 10^{4}$ m. The length of the active fiber in general is approximately a few meters, which is much shorter than the $Z_{\mathrm{walk-off}}$, so the mode bases are stable within the length of the active fiber. This point is also confirmed by our experiments; the corresponding experimental results are shown in Fig. 6(b).

As shown in Fig. 2(a), by taking an infinitesimal element in the cross section of the active fiber to establish the fluorescence emission model of localized analysis in few-mode active fibers, the amplification of the signal in the active fiber is regarded as the process of photon–electron interaction, and the process is represented by a two-level system composed of erbium ions composed of energy levels $^4\mathrm{I}_{11/2}$ (excited state energy level) and $^4\mathrm{I}_{15/2}$ (ground state energy level). As the pump field (980 nm) is injected into the active fiber, the electrons in the erbium ions in the ground state energy level reach the excited state level. The injection of the signal field (1550 nm) induces ions to reach the excited state energy level, after which the ions return to the ground-state energy level to release many photons to amplify the signal. However, the mode spatial intensity distributions between the LP and OAM modes of the same order

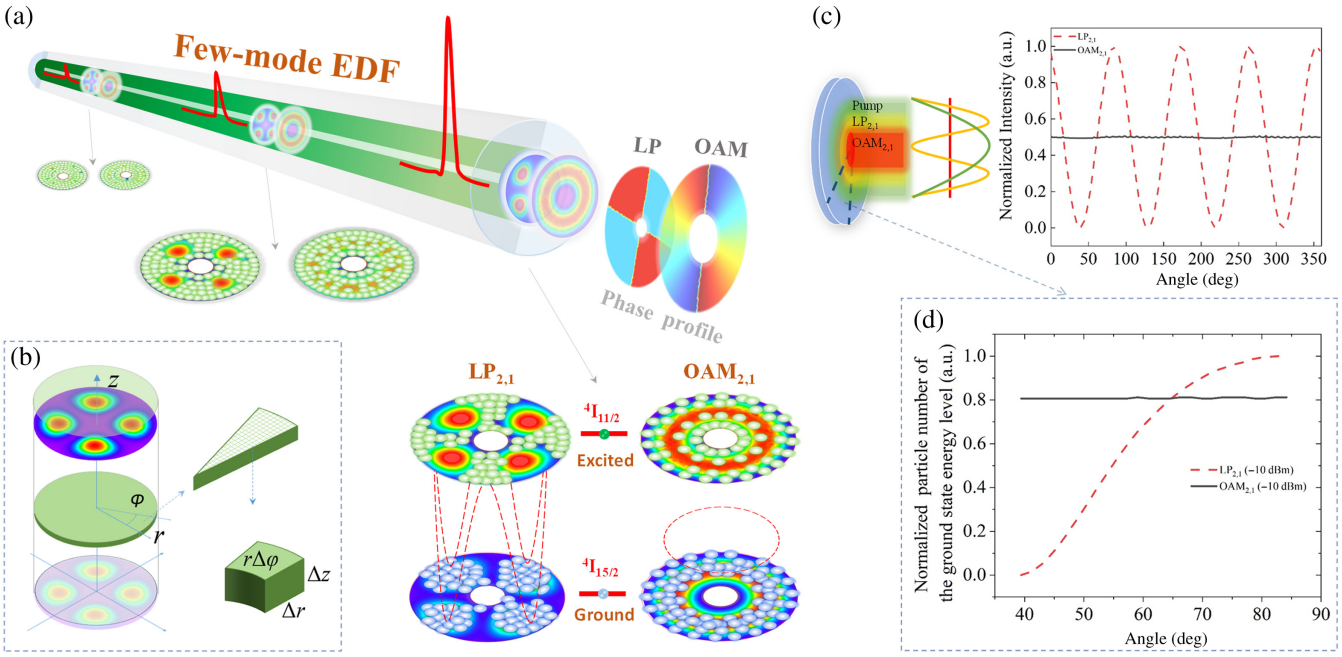

Fig. 2 LP and OAM mode fluorescence emission processes in an FM-EDF. (a) Energy-level structure model of a signal carrying photon excitation based on photon–electron interactions, and evolution of the inversion particle distribution in FM-EDF with respect to the fiber length; (b) local analysis model micro-elements in FM-EDF; (c) normalized intensity of the LP and OAM modes; and (d) local normalized particle number of the ground-state energy level.

radial mode exhibit local differences in azimuth, and the local differences in the mode spatial intensity distributions determine the local differences in the spatial photon number distributions, which leads to local gain differences. Moreover, Fig. 2(a) shows the evolution process of the distribution of $^4I_{11/2}$ and $^4I_{15/2}$ with different active fiber lengths. When the fiber is short, the number of particles of $^4I_{11/2}$ and $^4I_{15/2}$ of LP and OAM modes bases is the same; with the increase of fiber length, the number of particles of $^4I_{11/2}$ and $^4I_{15/2}$ will be different due to the difference of mode intensity distribution, and the number of particles of $^4I_{15/2}$ will be saturated at the high spatial intensity of the LP mode. However, the number of particles of $^4I_{15/2}$ uniformly increases, and there is no saturation phenomenon in the OAM modes.

To explain the difference in DMBG between the LP and OAM modes, we analyzed the two-state energy levels (excited state and ground state) of the particle number distribution via the established fluorescence emission process model. Here, we discretize the above model in the cross-sectional area, so that we can obtain a local analysis model composed of discrete elements of the FM-EDF cross section in the mode spatial intensity distribution azimuthal variation areas to clearly understand the particle number distribution at the cross section of the FM-EDF. Here, $N_1(r,\varphi,z)$ and $N_2(r,\varphi,z)$ represent the numbers of particles in the excited state and ground-energy levels, respectively. To better explore the distribution of $N_1(r,\varphi,z)$ and $N_2(r,\varphi,z)$, where r is the radial length of the fiber, φ is the azimuthal angle, and z is the fiber length, we build the localized analysis model shown in Fig. 2(b) using a micro-element (i.e., the difference in the spatial intensity distributions between the LP and OAM modes with azimuth angles within the same radius) in the FM-EDF cross section to analyze the distribution of N_1 and N_2 in the azimuth of the same radius. At the steady state, the excited energy level of the erbium ion concentration is expressed as[50–52]

$$N_2(r,\varphi,z)=\frac{\left[\frac{1}{hv_p}P_p(z)\sigma_{\mathrm{ap}}\Gamma_p+\frac{1}{hv_s}P_{s,i}(z)\sigma_{\mathrm{as}}\Gamma_{s,i}\right]N_0(r,\varphi,z)}{\frac{1}{hv_p}P_p(z)\sigma_{\mathrm{ap}}\Gamma_p+\frac{1}{hv_s}P_{s,i}(z)(\sigma_{\mathrm{as}}+\sigma_{\mathrm{es}})\Gamma_{s,i}+\frac{1}{\tau}}, \tag{2}$$

$$N_1(r,\varphi,z)=N_0(r,\varphi,z)-N_2(r,\varphi,z), \tag{3}$$

where $N_0(r,\varphi,z)$ represents the total concentration of erbium particles, v_s and v_p are the frequencies of the signal and pump, respectively, and h is Planck's constant. After the fiber material is determined, the radiation cross section and absorption cross section are only related to the wavelength and do not change with the distribution of erbium ions. σ_{as} and σ_{es} are the absorption cross-sectional area and radiation cross-sectional area, respectively; in the signal mode, σ_{ap} is the absorption cross-sectional area in pump mode, and τ is the lifetime of erbium ions in the FMF. Γ_p and $\Gamma_{s,i}$ are the power overlap integrals of pump and fluorescent photons, respectively, which are related to the intensity distribution of the pump and signal field. The signal power depends on the particle number distribution state of $N_1(r,\varphi,z)$ and $N_2(r,\varphi,z)$, and their rates are expressed as[50,52]

$$\frac{\mathrm{d}P_{\mathrm{signal},m}(z)}{\mathrm{d}z}=P_{\mathrm{signal},m}(z)\sum_k I_{s,m,k}(r,\varphi,z)\times[N_{2,k}(r,\varphi,z)\sigma_{\mathrm{es}}-N_{1,k}(r,\varphi,z)\sigma_{\mathrm{as}}], \tag{4}$$

$$\frac{\mathrm{d}P_{\mathrm{signal},m}(z)}{\mathrm{d}z}=P_{\mathrm{signal},m}(z)\sum_k I_{s,m,k}(r,\varphi,z)\times[N_{0,k}(r,\varphi,z)\sigma_{\mathrm{es}}-N_{1,k}(r,\varphi,z)(\sigma_{\mathrm{as}}+\sigma_{\mathrm{es}})], \tag{5}$$

where P_s are the fluorescence photon powers, which are the signal mode powers. Equation (5) can be obtained by substituting Eqs. (2) and (3) into Eq. (4). Equation (5) shows that the signal mode power can be affected only by N_1. Only the signal mode spatial intensity distribution can affect the distribution of N_1 with the same pump mode and power. In FM-EDFs, photons interact with dopant ions, and one of the critical processes is stimulated radiation absorption and emission. Areas with high-mode spatial intensity distributions have more photons. Conversely, areas with low-mode spatial intensity distributions have fewer photon populations. Due to the difference in the mode spatial intensity distributions of the LP and OAM modes, as shown in Fig. 2(c), there are local differences in N_1 during the amplification process in the FM-EDF. The spatial intensity distribution of the LP mode is sinusoidal, whereas the spatial intensity of the OAM mode is uniform. This is the main reason for generating DMBG in the FM-EDF. We will be able to better understand this difference in the distribution of N_1 by the localized analysis model shown in Fig. 2(d). Here, the azimuthal angle of 0 deg is the location of the high spatial intensity distribution, turning 360 deg counterclockwise in the fiber. We select the areas where the azimuthal angle ranges from 40 to 85 deg [i.e., the shaded area in Fig. 2(c)]. N_1 in the LP mode will be saturated in the high spatial intensity distribution areas, which means that the local gain of the LP mode will be saturated and not increase in this area. Moreover, N_1 in the OAM mode uniformly increases, and the local gain increases in the micro-element area, further illustrating the differences in gain between the LP and OAM modes.

This localized analysis model is proposed to deal with the gain details of the nonhomogeneous transverse distribution of signal mode intensity in the FM-EDF and to clarify the effect of the intensity difference caused by the difference of mode phase distribution on the overall gain. It does not put more restrictions on the fiber structure. In other words, this model can be used to describe the gain process of other types of active fibers in detail, as long as the intensity of the signal mode is distributed steadily over the gain process of concern.

3 Simulation Analysis

To better explain the DMBG caused by the different mode phase profiles, we use the localized analysis model shown in Fig. 2(c) to analyze the particle number distribution of N_1 from the following two aspects: signal power and fiber length. First, we analyze the influence of the signal power on the DMBG, as shown in Fig. 3(a). As the signal power increases, the distribution of N_1 at the difference in the mode spatial intensity distribution between the LP and OAM modes (from 40 to 85 deg of the azimuthal angle) will continue to increase. According to the analysis of Fig. 3(a), as the signal power increases, N_1 will increase until it reaches saturation because the mode spatial intensity distribution of the LP mode is a lobe shape, and N_1 reaches saturation in the high spatial intensity distribution area. However, the mode spatial intensity distribution of OAM modes is uniform, and N_1 also uniformly increases and does not reach

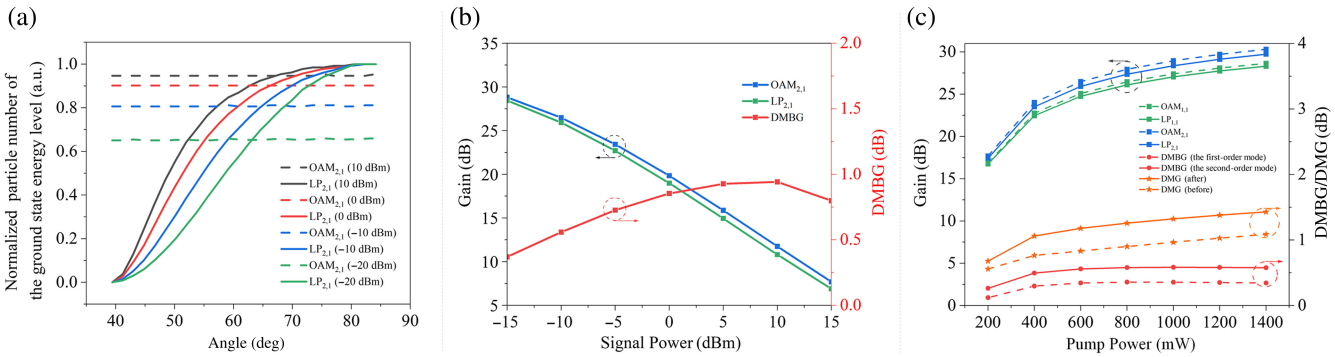

Fig. 3 Simulation results for different cases. (a) Lower-energy-level particle population distribution for a range of signal power (–20 to 10 dBm) with a pump power of 600 mW; (b) gain and DMBG of LP and OAM modes with a range of signal power from –15 to 15 dBm; and (c) modal gains of the second-order and first-order signals, DMBG, DMG before and after controlling the mode phase profile in the FM-EDF at a wavelength of 1550 nm with a signal power of –10 dBm as functions of the pump power.

saturation. As the difference in the local N_1 determines the local gain difference during the amplification process in the FM-EDF, the DMBG between the LP and OAM modes will occur. As shown in Fig. 3(b), when the signal power is set to −15 dBm, the DMBG is ∼0.37 dB, but when the signal power is set to 10 dBm, the DMBG is ∼0.95 dB, and as the signal power increases, the DMBG starts to decrease. As the signal power is low, the saturation range of N_1 in the LP mode is small. As the signal power increases, the saturated range of N_1 in the LP mode becomes increasingly larger. In the saturated area, the mode gain reaches a maximum and cannot further increase. As the saturated range of N_1 increases, the DMBG becomes increasingly larger as the range of mode gain also increases. When the signal power is close to the saturated output power, the distribution of N_1 decreases, and the DMBG decreases. Figure 3(c) shows the modal gains of the second- and first-order signals, DMBG and DMG, in FM-EDF at a wavelength of 1550 nm with a signal power of −10 dBm as a function of the pump power. Because of the presence of DMBG, we can use DMBG to improve the performance of the DMG and the saturated output power. By controlling the mode phase profile to switch $LP_{1,1}$ to $OAM_{1,1}$ modes, the DMG decreases by 0.35 dB from 1.37 to 1.02 dB, and the saturated output power of the first-order radial mode increases by 0.35 dB.

Similarly, the fiber length is also an important factor influencing the DMBG. As the active fiber length increases, the total number of doped particles in the active fiber increases, increasing the DMBG size. The total doped particle number in the FM-EDF determines the total group state particle number, which affects the gain of the FM-EDFA. Figure 4(a) shows the evolution of the particle number spatial distribution with the LP and OAM modes in the active fiber. As the active fiber length increases, the distribution of N_1 in the LP mode becomes saturated in the high spatial intensity distribution area. In contrast, the distribution of N_1 in the OAM mode uniformly increases and is not saturated. We choose representative fiber lengths (2 and 4 m) and analyze the distribution of N_1 as the difference in the mode spatial intensity distribution areas between the LP mode and OAM mode (from 40 to 85 deg of the azimuth angle). As shown in Fig. 4(b), as the active fiber length increases, the saturated area of N_1 in the LP mode continuously increases. Simultaneously, N_1 will not appear saturated but will constantly increase in the OAM mode. A longer active fiber length means a greater number of erbium particles. Thus, the number of erbium particles

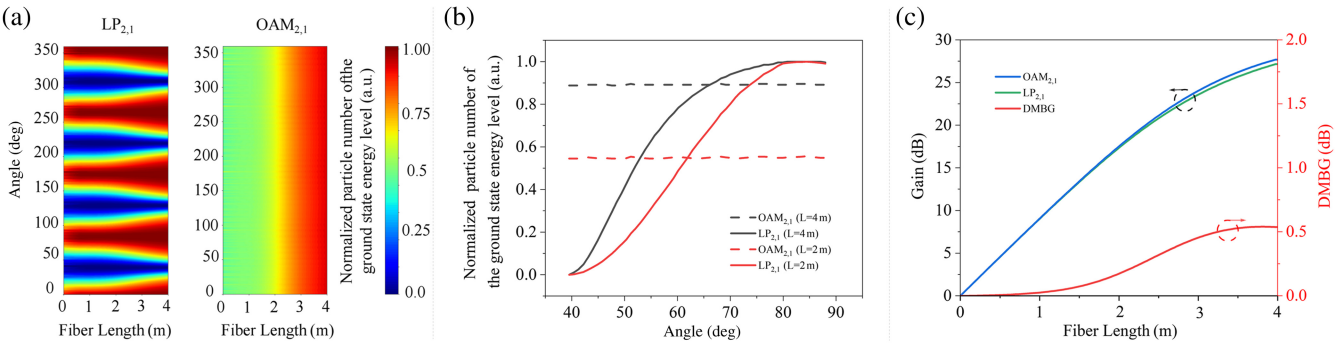

Fig. 4 (a) Evolution process of particles in the optical fiber as the length changes; (b) lower-energy-level particle population distribution of different fiber lengths of 2 and 4 m with a pump power of 600 mW; and (c) gain and DMBG of LP and OAM modes with different fiber lengths and a signal power of –10 dBm.

increases in the excited state, and the inversion particle number increases. However, due to the local saturation of N_1, further increasing the active fiber length cannot further increase N_1 at high spatial intensity distribution areas in LP modes, and as the saturated area of N_1 continues to increase, more local gains will stop increasing. In contrast, as N_1 in the OAM mode can continue to increase and not become saturated, the local gain will increase. The local distribution difference in N_1 causes the local mode gain difference between the LP and OAM modes, resulting in the DMBG, as shown in Fig. 4(c). As the active fiber length increases, the DMBG also increases to ~0.55 dB.

In the simulation analysis here, we assume that the distribution of erbium ions in the fiber is uniform, and the pump is a fundamental-mode core pump, but this analysis model is not limited to this, and it can also be used to analyze the situation of uneven transverse distribution of gain ions and arbitrary pumping mode.

4 Experimental Verification

The above simulation analysis revealed the reasons for the DMBG caused by the mode phase profile. To confirm the effect of the mode phase profile on the modal gain difference in the FM-EDFA, an FM-EDF is used, and a mode phase profile controlling a few-mode amplifier testing system based on space optical components is constructed. Figure 5(a) shows a microscope image of the cross-section of the used FM-EDF, whereas Fig. 5(b) represents its refractive index profile. The diameter of the FM-EDF core and the trench are 18 and 33 μm, respectively. The index differences between the fiber cores, the trench, and the cladding are 0.012 and 0.004, respectively. It can support the amplification of four modal groups (i.e., $LP_{0,1}$, $LP_{1,1}$, $LP_{2,1}$, and $LP_{0,2}$). Here, we focus on the two mode groups with higher azimuthal order, that is, the $LP_{1,1}(OAM_{1,1})$ and $LP_{2,1}(OAM_{2,1})$ modes; their phase and intensity distribution are illustrated in Fig. 5(c). A schematic of the mode phase profile can be regulated; the test experimental setup is shown in Fig. 5(d). The high-order signal is generated by launching the output of a tunable laser by loading a phase hologram on a spatial light modulator (SLM). The SLM is combined with the cascaded $\lambda/2$ and $\lambda/4$ plates to form a mode phase controller (MPC), which is used to control the mode phase profile[36,39] in the same order mode group excited in the FM-EDF. By controlling the MPC properly, the mode state in the FM-EDF between the LP and OAM mode bases can be switched. The collimator lens was used to couple the coaxial beam to the FM-EDF, and the end of the FM-EDF was angle-cleaved by 8 deg to suppress any undesired influence of the parasitic laser.[53] The dichroic mirror (DM) is used at the output end to filter out the remaining pump,[54] and the signal light is divided into two lights through beam splitters. On the one hand, an objective lens (Obj) is used to couple the amplified signal demodulated by the phase plate into a single-mode fiber and then connected to an optical spectrum analyzer through a single-mode fiber for recording after the amplification spectrum is obtained.[43] On the other hand, the modal intensity distribution of the output signal is observed by a charge-coupled device (CCD).

To experimentally test the difference in DMBG between the LP and OAM modes, we control the input signal mode phase profile using MPC to realize mode-bases switching. As the mode supported by the FM-EDF is up to the second-order mode, we test the mode gain of the first- and second-order modes with the same order radial vector mode group. During testing, the effective mode-bases amplification needs to be clarified. The LP and OAM modes are distinguished by observing the mode spiral interference via the CCD. Figure 6(a) shows the mode intensity distributions and interference patterns of the first- and second-order modes at a wavelength of 1550 nm under 150-mW total pump power, confirming the existence of two modes (LP and OAM modes) in the FM-EDF. The propagation

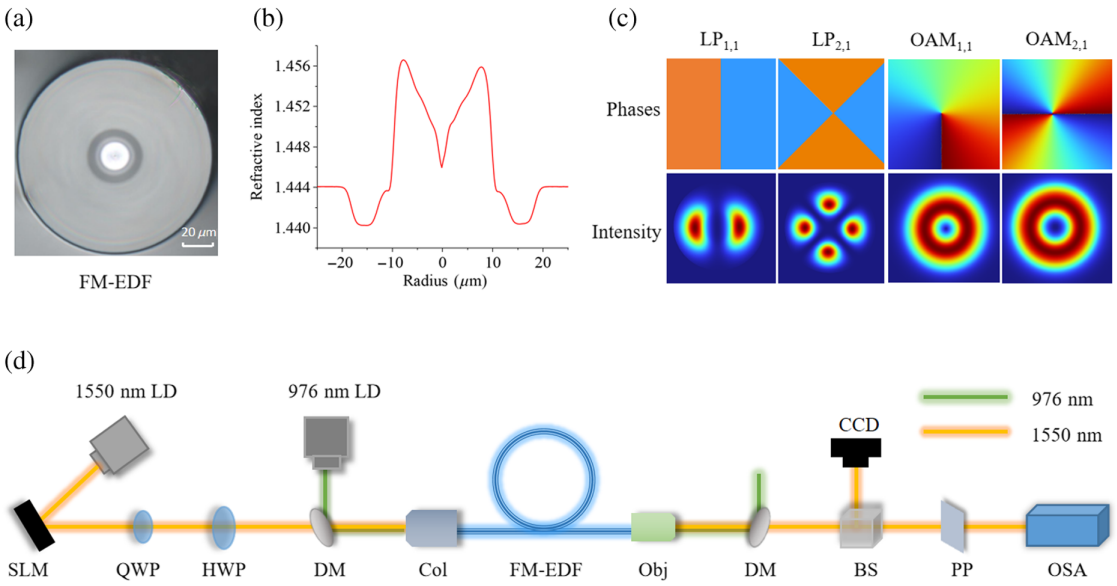

Fig. 5 (a) Cross section, (b) refractive index profile, and (c) calculated mode phase and intensity distribution of the FM-EDF used. (d) Experimental optical test system setup for the gain test based on space optical components. SLM, spatial light modulator; QWP, quarter-wave plate; HWP, half-wave plate; Col, collimator; DM, dichroic mirror; BS, beam splitter; Obj, objective lens; PP, phase plate; CCD, charge-coupled device; OSA, optical spectrum analyzer.

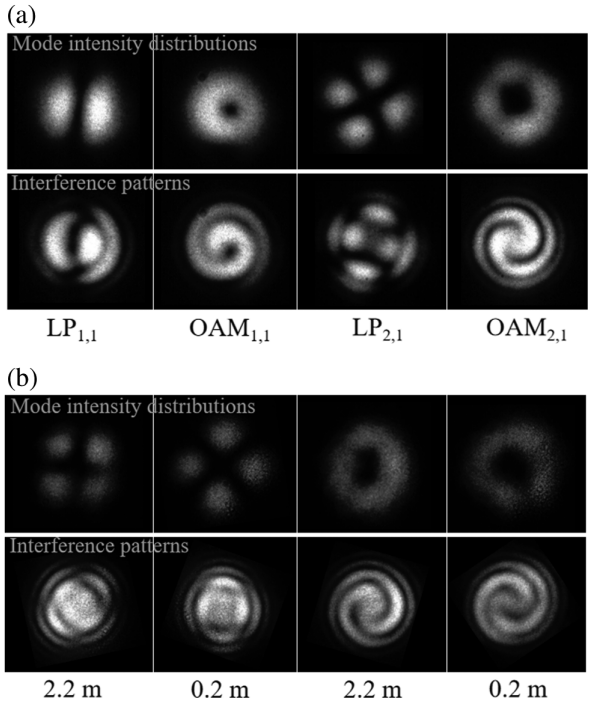

Fig. 6 (a) Modal intensity distributions and interference patterns of the first- and second-order signal modes at a wavelength of 1550 nm under 150-mW total pump power and (b) modal intensity distributions and interference patterns obtained by shortening the fiber length from 2.2 to 0.2 m.

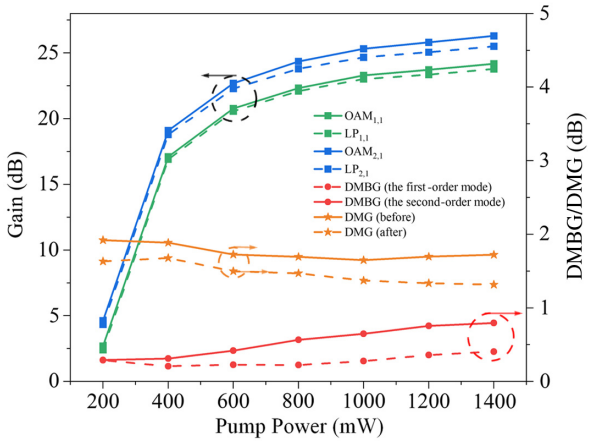

Fig. 7 Measured modal gains of the second- and first-order signals, DMBG, and DMG before and after controlling the mode phase profile in the FM-EDF at a wavelength of 1550 nm with a signal power of −10 dBm as functions of the pump power.

stability is another critical factor that influences effective mode-bases amplification. Therefore, we observe whether the mode bases change by shortening the fiber length from 2.2 to 0.2 m to verify the mode propagation stability in the active fiber. The results are shown in Fig. 6(b) that the mode propagation is stable over the length of the FM-EDF.

Moreover, the signal modal gain of the FM-EDF is measured by launching the LP and OAM modes at 1550 nm and pump powers ranging from 200 to 1400 mW. Considering the various losses from the input to the output on the spatial optical path, we obtained the corresponding mode gain, DMBG, and comparison of DMG in the different pump powers; the results are shown in Fig. 7. As the pump power increases, the DMBG of the second-order mode increases from 0.40 to 0.80 dB, with a signal power of −10 dBm. When the DMBG becomes increasingly larger because the local mode gain simultaneously saturates, the DMBG of the first-order mode is 0.40 dB, which is smaller than the DMBG of 0.80 dB of the second-order mode at a pump power of 1400 mW and a signal power of −10 dBm. Using the MPC to control the mode phase profile to switch $LP_{1,1}$ mode to $OAM_{1,1}$ mode, the performance of FM-EDFA can be improved at a pump power of 1400 mW and signal power of −10 dBm. The DMG decreases by ∼0.40 dB from 1.72 to 1.32 dB, and the saturated output power of the first-order mode increases by ∼0.40 dB.

To verify the simulation results, the signal modal gain test and DMBG are measured by launching the LP and OAM modes at 1550 nm with a range of signal power from −15 to 15 dBm in the FM-EDF. The results are shown in Fig. 8(b). When the signal power is set to −15 dBm, the DMBG is ∼0.15 dB, but when the signal power is set to 10 dBm, the DMBG is ∼1.2 dB, and as the signal power increases, the DMBG starts to decrease. This result verifies the simulation results. We also recorded the changes in the modal intensity distributions of the LP and OAM modes for a range of signal power from −10 to 10 dBm via a CCD. Figure 8(a) shows the mode spatial intensity distributions for a range of signal power between the LP and OAM modes. As the signal power increases, the local modal gain of the LP mode is saturated in the high-mode spatial intensity distribution areas. However, there are still some areas that are not saturated in the low spatial intensity distribution area in the OAM mode, and the local modal gain of the OAM mode uniformly increases. Because of the difference in local mode gain between the LP and OAM modes, the DMBG can be generated in the FM-EDFA. These results demonstrate that the DMBG can be used to reduce the DMG of modes among different mode groups by combining different mode bases.

5 Conclusion

We constructed a discrete pixelated local analysis model for the FM-EDF to accurately characterize the local gain of signal mode in detail and then obtained the overall mode gain difference between the LP and OAM mode bases. Using this local analysis model, we described the gain details of two mode bases, analyzed the particle number distribution during the amplification process in the FM-EDF, and obtained the overall gain difference between the two mode bases. Moreover, this model was used to explain the reasons for DMBG by analyzing the distribution of N_1 with different signal powers and fiber lengths. These two aspects reflect the phenomenon in which the local distribution of N_1 reaches saturation, which is caused by the local mode gaining saturation. We also constructed an amplifying testing system based on controlling the mode phase profile to characterize the gain of two different phase profile modes and experimentally confirmed the simulation results. This proposed model can also be used to describe the gain process of other types of active fibers with an uneven transverse distribution of gain ions under the arbitrary distribution of pump modes. The DMBG found in this work not only provides a new strategy to equalize the DMG in the FM-EDFA but also gives a way to

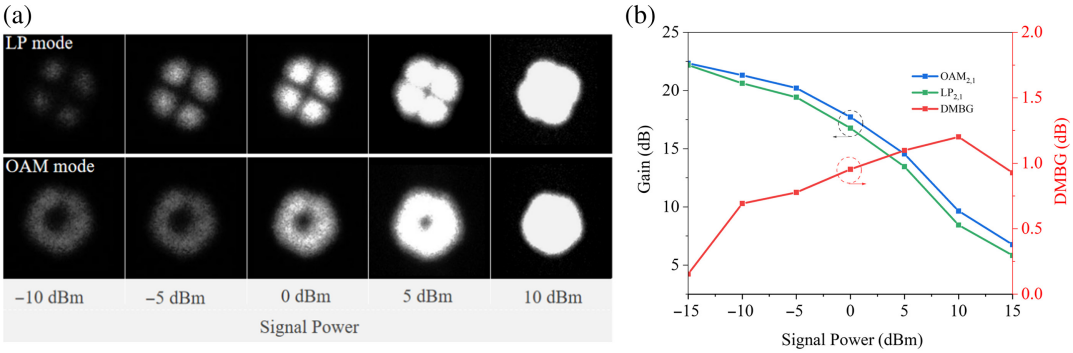

Fig. 8 (a) Modal intensity distributions of the LP (top row) and OAM modes (bottom row) with a range of signal power from −10 to 10 dBm at a wavelength of 1550 nm under 300-mW total pump power. (b) Measured modal gain of the second-order signal between the LP and OAM modes in the FM-EDF under amplification at a 1550-nm wavelength with a range of signal power from −15 to 15 dBm; the red line represents the DMBG.

improve the saturation gain of the FM-EDFA. This is significant for optimizing the amplification in long-distance MDM communications.

Disclosures

The authors declare no conflicts of interest.

Code and Data Availability

The data that support the findings of this paper are available from the corresponding author upon reasonable request.

Acknowledgments

This work was supported by the National Key Research and Development Program of China (Grant No. 2019YFA0706300), the National Natural Science Foundation of China (Grant Nos. U22B2010, 62035018, and U2001601), the Program of Marine Economy Development Special Fund (Six Marine Industries) under the Department of Natural Resources of Guangdong Province (Grant No. GDNRC [2024]16), and the project supported by the Southern Marine Science and Engineering Guangdong Laboratory (Zhuhai) (Grant No. SML2023SP231).

References

1. D. J. Richardson, J. M. Fini, and L. E. Nelson, "Space-division multiplexing in optical fibres," *Nat. Photonics* **7**(5), 354–362 (2013).
2. K. Zou et al., "High-capacity free-space optical communications using wavelength-and mode-division-multiplexing in the mid-infrared region," *Nat. Commun.* **13**(1), 7662 (2022).
3. P. Sillard et al., "Few-mode fiber technology, deployments, and systems," *Proc. IEEE* **110**(11), 1804–1820 (2022).
4. B. J. Puttnam, G. Rademacher, and R. S. Luís, "Space-division multiplexing for optical fiber communications," *Optica* **8**(9), 1186–1203 (2021).
5. G. Li et al., "Space-division multiplexing: the next frontier in optical communication," *Adv. Opt. Photonics* **6**(4), 413–487 (2014).
6. A. Ferrari, E. Virgillito, and V. Curri, "Band-division vs. space-division multiplexing: a network performance statistical assessment," *J. Lightwave Technol.* **38**(5), 1041–1049 (2020).
7. C. Huang et al., "High-capacity space-division multiplexing communications with silicon photonic blind source separation," *J. Lightwave Technol.* **40**(6), 1617–1632 (2022).
8. Y. Tian et al., "Wavelength-interleaved MDM-WDM transmission over weakly coupled FMF," *Opt. Express* **25**(14), 16603–16617 (2017).
9. J. Zhang et al., "Mode-division multiplexed transmission of wavelength division multiplexing signals over a 100-km single-span orbital angular momentum fiber," *Photonics Res.* **8**(7), 1236–1242 (2020).
10. Y. Xie et al., "Design and characterization of nanopore-assisted weakly-coupled few-mode fiber for simpler MIMO space division multiplexing," *IEEE Access* **8**, 76173–76181 (2020).
11. Z. Liu et al., "Broadband, low-crosstalk, and massive-channels OAM modes de/multiplexing based on optical diffraction neural network," *Laser Photonics Rev.* **17**(4), 2200536 (2023).
12. J. Liu et al., "1-Pbps orbital angular momentum fibre-optic transmission," *Light Sci. Appl.* **11**(1), 202 (2022).
13. J. Zhu et al., "Weakly-coupled MDM-WDM amplification and transmission based on compact FM-EDFA," *J. Lightwave Technol.* **38**(18), 5163–5169 (2020).
14. Z. Li et al., "Amplification and transmission system with matching multilayer ion-doped FM-EDFA," *J. Lightwave Technol.* **41**(2), 695–701 (2022).
15. H. Guo et al., "Few-mode erbium-doped fiber amplifier with high gain and low differential modal gain for mode-division-multiplexed systems," *J. Lightwave Technol.* **41**(21), 6657–6663 (2023).
16. N. Bai et al., "Mode-division multiplexed transmission with inline few mode fiber amplifier," *Opt. Express* **20**(3), 2668–2680 (2012).
17. R. N. Mahalati, D. Askarov, and J. M. Kahn, "Adaptive modal gain equalization techniques in multi-mode erbium-doped fiber amplifiers," *J. Lightwave Technol.* **32**(11), 2133–2143 (2014).
18. L. Bigot, G. Le Cocq, and Y. Quiquempois, "Few-mode erbium-doped fiber amplifiers: a review," *J. Lightwave Technol.* **33**(3), 588–596 (2015).
19. Z. Li et al., "A multi-layer erbium-doped air-hole-assisted few-mode fiber with ultra-low differential modal gain," *Photonics* **9**(5), 305, (2022).
20. Q. Zhao et al., "Demonstration of a ring-core few-mode erbium-doped fiber for mode gain equalization based on layered doping," *JOSA B* **39**(7), 1972–1978 (2022).
21. W. Xu et al., "Gain characteristics of few-mode EDFA with different pump," *IEEE Photonics J.* **14**(5), 1–7 (2022).
22. Z. Li et al., "Hybrid-pumped few-mode erbium-doped fiber amplifier for gain equalization," *IEEE Photonics Technol. Lett.* **35**(18), 971–974 (2023).
23. J.-B. Trinel et al., "Latest results and future perspectives on few-mode erbium doped fiber amplifiers," *Opt. Fiber Technol.* **35**, 56–63 (2017).

24. Q. Qiu et al., "High power-efficiency, low DMG cladding-pumped few-mode Er/Yb/P co-doped fiber amplifier for mode division multiplexing," *J. Lightwave Technol.* **40**(22), 7421–7430 (2022).
25. C. Zhang et al., "Differential mode-gain equalization via femtosecond laser micromachining-induced refractive index tailoring," *Light Adv. Manuf.* **5**, 14 (2024).
26. C. Matte-Breton et al., "Modeling and characterization of cladding pumped erbium-ytterbium co-doped fibers for amplification in communication systems," *J. Lightwave Technol.* **38**, 1936–1944 (2020).
27. H. Takeshita et al., "Configurations of pump injection and reinjection for improved amplification efficiency of turbo cladding pumped MC-EDFA," *J. Lightwave Technol.* **38**(11), 2922–2929 (2020).
28. J. Wang et al., "Terabit free-space data transmission employing orbital angular momentum multiplexing," *Nat. Photonics* **6**(7), 488–496 (2012).
29. N. Bozinovic et al., "Terabit-scale orbital angular momentum mode division multiplexing in fibers," *Science* **340**(6140), 1545–1548 (2013).
30. L. Zhu et al., "Experimental demonstration of linearly polarized (lp) modes and orbital angular momentum (OAM) modes conversion in few-mode fiber," in *Asia Commun. and Photonics Conf.*, Optica Publishing Group, p. ASu2A–98 (2015).
31. J. Wang and X. Zhang, "Orbital angular momentum in fibers," *J. Lightwave Technol.* **41**(7), 1934–1962 (2022).
32. M. van den Hout et al., "Transmission of 273.6 Tb/s over 1001 km of 15-mode multi-mode fiber using c-band only 16-qam signals," *J Lightwave Technol.* **42**(3), 1136–1142 (2023).
33. G. Rademacher et al., "Peta-bit-per-second optical communications system using a standard cladding diameter 15-mode fiber," *Nat. Commun.* **12**(1), 4238 (2021).
34. T. Xu et al., "High-gain integrated in-line few-mode amplifier enabling 3840-km long-haul transmission," *Photonics Res.* **10**(12), 2794–2801 (2022).
35. S. Fu et al., "Orbital angular momentum comb generation from azimuthal binary phases," *Adv. Photonics Nexus* **1**, 016003 (2022).
36. H. Wang et al., "Finding the superior mode basis for mode-division multiplexing: a comparison of spatial modes in air-core fiber," *Adv. Photonics* **5**, 056003 (2023).
37. L. Allen et al., "Orbital angular momentum of light and the transformation of Laguerre-Gaussian laser modes," *Phys. Rev. A* **45**(11), 8185 (1992).
38. S. Ramachandran and P. Kristensen, "Optical vortices in fiber," *Nanophotonics* **2**(5–6), 455–474 (2013).
39. S. Li et al., "Controllable all-fiber orbital angular momentum mode converter," *Opt. Lett.* **40**(18), 4376–4379 (2015).
40. L. Feng et al., "All-fiber generation of arbitrary cylindrical vector beams on the first-order poincaré sphere," *Photonics Res.* **8**(8), 1268–1277 (2020).
41. Y. Li et al., "Superposing multiple LP modes with microphase difference distributed along fiber to generate OAM mode," *IEEE Photonics J.* **9**(2), 1–9 (2017).
42. H. Zhang et al., "Generation of orbital angular momentum modes using fiber systems," *Appl. Sci.* **9**(5), 1033 (2019).
43. T. Wen et al., "Third-and fourth-order orbital angular momentum multiplexed amplification with ultra-low differential mode gain," *Opt. Lett.* **46**(21), 5473–5476 (2021).
44. J. Wang et al., "Tailoring light on three-dimensional photonic chips: a platform for versatile OAM mode optical interconnects," *Adv. Photonics* **5**, 036004 (2023).
45. A. Afanasev et al., "Nondiffractive three dimensional polarization features of optical vortex beams," *Adv. Photonics Nexus* **2**, 026001 (2023).
46. H. Guo et al., "Ultra-low-loss all-fiber orbital angular momentum mode division multiplexer based on cascaded fused-biconical mode selective couplers," *Adv. Photonics Nexus* **3**, 016006 (2024).
47. Z. Ma and S. Ramachandran, "Propagation stability in optical fibers: role of path memory and angular momentum," *Nanophotonics* **10**(1), 209–224 (2020).
48. Y. Yue et al., "Mode properties and propagation effects of optical orbital angular momentum (OAM) modes in a ring fiber," *IEEE Photonics J.* **4**(2), 535–543 (2012).
49. B. Mao et al., "Complex analysis between CV modes and OAM modes in fiber systems," *Nanophotonics* **8**(2), 271–285 (2018).
50. A. Saleh et al., "Modeling of gain in erbium-doped fiber amplifiers," *IEEE Photonics Technol. Lett.* **2**(10), 714–717 (1990).
51. Y. Xu et al., "Experimental measurement of absorption coefficients for effective erbium-doping concentration to optimize few-mode erbium-doped fiber amplifiers with low differential mode gain," *Photonics* **8**(6), 185, (2021).
52. J. Ma et al., "Amplification of 18 OAM modes in a ring-core erbium-doped fiber with low differential modal gain," *Opt. Express* **27**(26), 38087–38097 (2019).
53. Y. Jung et al., "Optical orbital angular momentum amplifier based on an air-hole erbium-doped fiber," *J. Lightwave Technol.* **35**(3), 430–436 (2017).
54. J. Liu et al., "Amplifying orbital angular momentum modes in ring-core erbium-doped fiber," *Research* **2020**, 762375 (2020).

Biographies of the authors are not available.